Ab initio molecular dynamics study of $CaSiO_3$ perovskite at *P-T* conditions of Earth's lower mantle

Donat J. Adams* and Artem R. Oganov
Laboratory of Crystallography, Department of Materials, ETH Honggerberg, Wolfgang-Pauli-Strasse 10, CH-8093 Zurich, Switzerland
(Received 23 December 2005; revised manuscript received 16 February 2006; published 4 May 2006)

First-principles molecular dynamics calculations were performed in order to investigate the structure and properties of what is thought to be the third most abundant phase in the Earth's lower mantle, $CaSiO_3$ perovskite. The commonly assumed cubic structure was found to be stable at high temperatures ($T > 1000-2000$ K) and unstable at low temperatures at all pressures. For this structure we investigate the thermal equation of state and the Grüneisen parameter. We predict that the ground state of $CaSiO_3$ perovskite is tetragonal (space group $I4/mcm$). At room temperature an orthorhombic structure (space group *Imma*) is possible, which explains puzzling experimental X-ray powder diffraction patterns. We consider the structure relation between the *Imma* and the $I4/mcm$ structures and show that the *Imma* structure can be obtained by a counterintuitive symmetry-lowering transition on increasing temperature.

DOI: 10.1103/PhysRevB.73.184106 PACS number(s): 61.50.Ks, 64.70.Kb, 66.10.Ed, 61.50.Ah

I. INTRODUCTION

$CaSiO_3$ perovskite is thought to comprise between 6 and 12 wt % of the lower half of the Earth's transition zone and lower mantle.[1,2] Its structure throughout the mantle *P-T* regime is generally assumed to be cubic.[3–6] In early experimental studies[5–7] $CaSiO_3$ perovskite appeared to have a cubic structure up to 134 GPa at room temperature. Recently, using higher-resolution experimental techniques, Shim *et al.* showed that temperature-quenched $CaSiO_3$ perovskite had a tetragonal symmetry from 20 to 46 GPa at room temperature.[8] These findings were confirmed by Ono *et al.*[9] and Kurashina *et al.*[10] who did experiments in the range from 38 GPa to 106 GPa and 300 K to 2600 K, and 24 GPa to 75 GPa and 300 K to 2250 K, respectively. Both studies agree that for the pure $CaSiO_3$ perovskite the phase transition to the high-temperature phase at around 50 GPa takes place between 500 K and 700 K with a Clapeyron slope of $\sim$180 MPa/K.

All-electron linearized-augmented plane wave (LAPW)-local-density approximation (LDA) calculations indicate that at low temperatures $CaSiO_3$ perovskite should have the $I4/mcm$ symmetry.[11] According to other calculations[12,13] $CaSiO_3$ perovskite would have an orthorhombic *Pbnm* symmetry at low temperatures. Pseudopotential LDA calculations[14,15] found the cubic ($Pm3m$) structure stable at 0 K, whereas more recent LDA pseudopotential calculations[16] and all-electron projector-augmented wave (PAW) generalized gradient approximation (GGA) calculations[17] find the $I4/mcm$ structure to be thermodynamically stable for $CaSiO_3$ perovskite at low temperatures. However, the $I4/mcm$ structure is in conflict with experiment. The lattice constants a and c from experiments for the cubic subcell[18] give a c/a ratio of 0.993,[9] whereas computations find $c/a=1.014$.[17] Shim *et al.* refined the structure in the $P4/mmm$ ($c/a=0.966$, octahedra not tilted) and the $I4/mmm$ ($c/a<1, a^0\beta^+\beta^+$) space groups.[8] The $P4/mmm$ structure can be ruled out, because in our calculations it does not correspond to an energy minimum, while the $I4/mmm$ is unlikely because it is higher in energy than the $I4/mcm$ by 3 meV/atom.[16] In this work using static energy minimization and molecular dynamics (MD) calculations, we investigate the ground state structure $CaSiO_3$ perovskite and—by considering temperature-driven phase transitions—address the controversy between previous studies.

In addition, we explored the possibility of fast ionic conductivity in $CaSiO_3$ perovskite. The mysterious mechanism of the electrical conductivity in the lower mantle that is needed to explain the modulation of the Earth's magnetic field is an open question.[19] Using classical MD simulations, Matsui and Price predicted that $MgSiO_3$ perovskite—due to diffusion of O^{2-} ions—can become an ionic conductor at high T when a cubic perovskite structure is formed.[20] Subsequent *ab initio* MD simulations[21] did not confirm the existence of cubic $MgSiO_3$ perovskite at mantle conditions. $CaSiO_3$, on the contrary, does adopt the cubic perovskite structure at all mantle conditions, which prompts the question about its possible ionic conductivity due to fast ionic diffusion.

II. METHODOLOGY

The Vienna *Ab Initio* Simulation Package (VASP)[22] has been used for MD simulations and structural optimization, based on the generalized gradient approximation (GGA)[23] and the all-electron projector-augmented wave (PAW) method.[24–26] In all calculations we have used the following PAW potentials for the atoms, all derived within the same GGA functional:[23] core region cutoffs are 2.3 a.u. for Ca (core configuration $1s^22s^2p^6$), 1.5 a.u. for silicon (core configuration $1s^22s^22p^6$) and 1.52 a.u. for oxygen (core configuration $1s^2$). This gives ten, four, and six electrons for the calcium, silicon, and oxygen atoms respectively, which have been explicitly treated. It is very important to take into account so many electrons for Ca because semicore states in this element ($3s,3p$) are known to play a significant role.[26] Partial core corrections were done for Ca and Si with partial core radii 2.0 a.u. and 1.30 a.u. respectively. Plane wave ki-

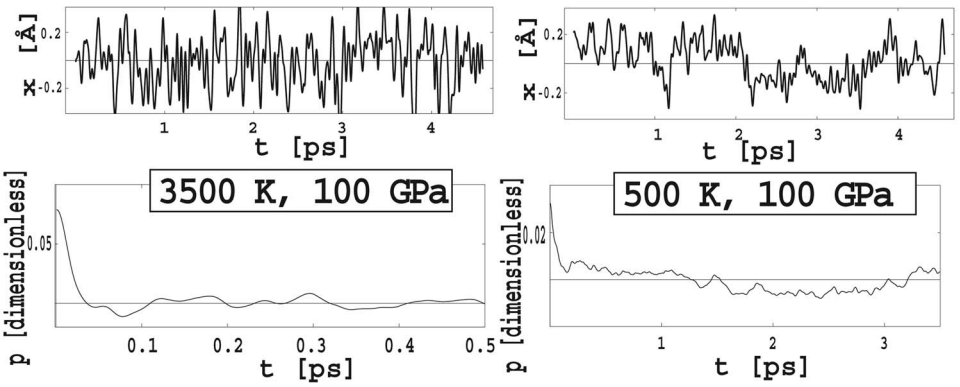

FIG. 1. Deviation of a coordinate of one oxygen atom from its mean in the ideal cubic structure as a function of simulation time and position correlation function of the same ion. The structure undergoes a phase transition between 1000 K and 500 K. This is reflected by the autocorrelation function decaying slowly in the case $T<1000$ K.

netic energy cutoff of 400 eV was used in our MD calculations.

The $CaSiO_3$ cubic structure (for which we used the 20 atoms unit cell) was first optimized at 0 K and pressures of 0 GPa, 50 GPa, 100 GPa, and 150 GPa. Here, we used the results of Jung and Oganov, obtained using the same methodology but with a higher plane-wave cutoff of 500 eV.[17] The structure was statically (0 K) relaxed with the conjugate gradients and the steepest descent methods. The self-consistency threshold for electronic optimization was 10^{-9} eV per 20 atoms cell; structural relaxation proceeded until the total energy changes were below 10^{-6} eV per cell. Later these optimized lattice parameters were combined with temperatures of 500, 1500, 2500, and 3500 K to perform MD simulations in the constant-*NVT* ensemble using the Nosé thermostat.[27] The $2\times2\times1$ supercell (80 atoms) used here includes tetragonal, orthorhombic, and cubic structures. Simulations were run for at least 8 ps with 1 fs time step. Equilibration lasted typically several hundred fs. At each time step the electrons were relaxed to the ground state with a self-consistency threshold of 2×10^{-5} eV.

For the Brillouin zone sampling we used only the Γ-point, which is sufficiently accurate for such large supercells and enables fast calculations. We checked convergence with respect to supercell size by simulating a larger supercell containing 160 atoms at 2500 K and 100 GPa. The Grüneisen parameter results on an 80-atom cell differ from those on a 160-atom cell by less than 1%.

Hydrostaticity of the calculated stress tensor was used as an indicator of phase transitions using the following idea: if a constant-volume simulation is performed in a supercell the shape of which does not reflect the correct symmetry, the stress tensor will likely be nonhydrostatic. For example, a noncubic structure put into a cubic cell exerts a stress on the faces of the supercell because the atoms energetically would prefer a different shape of the supercell. If we start with *P-T* conditions where $CaSiO_3$ perovskite has a cubic structure and slowly change the *P-T* conditions of the simulations, we will observe a phase transition as soon as the stress tensor becomes nonhydrostatic.

In MD simulations, stresses oscillate with time and only the time-averaged stresses have a physical meaning. We averaged stress tensor components over time of the MD simulations getting also the uncertainty in stresses $\Delta\sigma_i$ (of course, averaging was performed after sufficient time was given for equilibration). Errors in stress

$$\Delta\sigma_j = \frac{\langle\sigma_j^2\rangle - \langle\sigma_j\rangle^2}{\sqrt{\tau M/2\tau_j}}$$

were determined using the correlation time τ_j, the number of steps M and the step size τ (1 fs).[28] The correlation time τ_j was determined by the first zero of the autocorrelation function $\chi_i(t')=\lim_{T\to\infty}\frac{1}{T}\int_T\sigma_i(t)\cdot\sigma_i(t+t')dt$. This procedure resulted in reasonable correlation times of 20 to 30 fs at 3500 K and 60 to 300 fs at 500 K and error bars of 0.4–0.6 GPa at 3500 K and 0.2–1.5 GPa at 500 K.

For the comparison of stresses in different spatial directions in the MD runs, corrections using calculations at 0 K have been made. The need for such a correction comes form the fact that the 80-atoms supercell has different lengths along a, b, c directions ($a=b=c\sqrt{2}$) and therefore the density of reciprocal space sampling is different in different directions. This produces a small artificial nonhydrostaticity that needs to be removed from analysis. It was assumed that the errors coming from real space projection, finite basis set (Pulay stress) and k-point sampling are temperature independent at constant volume. For the high-precision calculation at 0 K (on the same 80-atom cell) we used k-point mesh $4\times4\times4$ and an energy cutoff of 500 eV. Stresses from these calculations were compared with stresses from the lower-cost calculations with only Γ-point and an energy cutoff of 400 eV, which is the same setting as for high-temperature calculations. Differences in stress between these calculations (typically, 5 GPa in a and b directions and 7 GPa in the c direction) were added to the average stresses from high-temperature calculations; such a correction was calculated for each simulated volume.

Yet another indicator for a phase transition was used. The position correlation function $p_i(t)=\langle(r_i(t+t_0)-R_i^0)\cdot(r_i(t_0)-R_i^0)\rangle$ and the correlation time τ_i^a for the movement of individual atoms was used by Vocadlo *et al.* to predict phase transitions in iron at extreme conditions.[29] Here the superscript a indicates the correlation time for atomic movement,

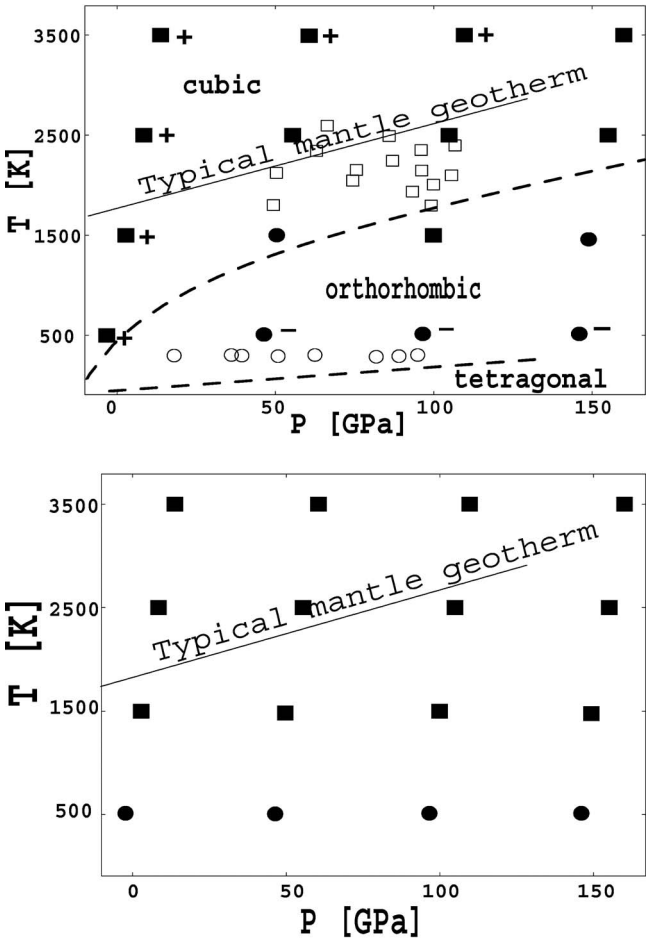

FIG. 2. (a) Phase diagram of Ca-perovskite using analysis of differences in stress. Filled symbols (●,■) from theory (this work), open symbols (□,○) from experiment (Ref. 42). Squares stand for the cubic structure, circles for the low temperature structure. Correlation (+) and anticorrelation (−) between any two of the stress components in the simulation are also indicated. The dashed lines are estimated phase boundaries. The phase boundary between the cubic and the orthorhombic phases is estimated from differences in stress in the MD runs. The phase boundary between the orthorhombic and the tetragonal phases is estimated from the enthalpy difference between the two structures ($T_c \approx \Delta H/k_B$, $\Delta H=1$ meV at 0 GPa, $\Delta H=17$ meV at 100 GPa). Error bars on these lines are expected to be big because of statistics and relatively big temperature increment in the simulations. (b) Phase diagram of Ca-perovskite using position correlation function of oxygen atoms as an indicator for a phase transition.

which is different for the correlation time for the oscillations of the stress tensor. We defined the correlation time τ_i^a by the first zero of the position correlation function (for details see Fig. 1). Since the expected phase transition occurs by rotations of nearly rigid SiO_6 octahedra, the largest displacement upon transition should be for the oxygen atoms on which we focused our analysis. Their correlation time gives an estimate of the lifetime of octahedral tiltings. We compare the correlation time of oxygen atoms with the average vibrational period τ_{vib} (~50 fs) obtained from phonon calculations of Ref. 16. If the average correlation time of the oxygen atoms is significantly higher than the average vibrational period (i.e., $\langle \tau_i^a \rangle > \tau_{vib} \cdot 5$), we conclude that a phase transition from the cubic to a lower-symmetry phase has occurred. The results are given in Fig. 2(b).

We performed static simulations for the same $2\times2\times1$ supercell and with the same computational conditions; at each temperature the thermal pressure was obtained as the difference of pressures in the static and thermal system,

$$P_{vib}(V,T) = P(V,T) - P_{st}(V), \tag{1}$$

where $P(V,T)$ includes the kinetic gas correction $(N-1)k_BT/V$, where N is the number of atoms in the system.

Following Oganov and Dorogokupets, we define the effective Grüneisen parameter,[30]

$$\gamma_{eff}(V,T) = \frac{P_{vib}(V,T)}{(3N-3)k_BT}. \tag{2}$$

For a quasiharmonic classical solid the Grüneisen parameter depends only on volume but due to intrinsic anharmonicity the actual $\gamma_{eff}(V,T)$ has a small temperature dependence from which intrinsic anharmonic effects can be extracted.[30]

III. RESULTS

A. Phase diagrams

Starting with high temperatures, we expected the atoms to exert different stresses on different surfaces of the box as temperature was lowered. As we observe a significant ($|\sigma_i - \sigma_j| > 3\Delta\sigma_{ij}$, $\Delta\sigma_{ij} = \Delta\sigma_i + \Delta\sigma_j$) difference in stress components, we predict that a transition takes place between 1000 K and 2000 K [Fig. 2(a)]; thus we confirm that the high-temperature cubic phase is stable at the conditions of the Earth's lower mantle.

For the phase transition a second indicator was introduced: the cross correlation between the stress components $r_{ij} = \frac{\langle(\sigma_i(t)-\sigma_i^0)\cdot(\sigma_j(t)-\sigma_j^0)\rangle}{\langle(\sigma_i(t)-\sigma_i^0)\rangle\cdot\langle(\sigma_j(t)-\sigma_j^0)\rangle}$ where σ_j^0 are the averaged stresses. r_{ij} equals 1 if the two components have a correlated time development, and it equals −1 if the time development is anticorrelated. Correlation and anticorrelation are considered to be significant when $|r_{ij}| > \frac{1}{3}$. Correlation of the stress components appears to be present for cubic symmetry [see Fig. 2(a)]. Anticorrelation can be explained by a switching of the tilting direction on the picosecond time scale: during the MD run, the structure exerts smaller pressure in the directions perpendicular to the tilting axis. In a macroscopic crystal the time scale of such a switching may diverge to infinity.

1. Symmetry of high-temperature $CaSiO_3$

For symmetry determination, atomic positions were averaged over a whole run after equilibration. Thus at high temperatures and all pressures, we observe a cubic phase with negligible octahedral tilting angles; e.g., at 3500 K and 100 GPa, the tilting angles are $\alpha = 0.25 \pm 0.27°$, $\beta = 0.15 \pm 0.19°$, $\gamma = 0.44 \pm 0.54°$ (Fig. 3).[31] This leads to an undistorted average cubic $Pm3m$ symmetry at high temperatures and high pressures.

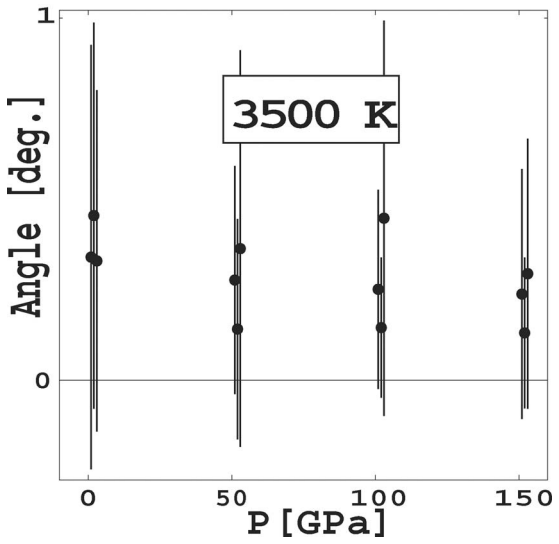

FIG. 3. Tilting angles at 3500 K and pressures of 0 to 150 GPa. Data points are well below 1° and error bars from statistics over 16 octahedra are relatively big. This indicates a cubic structure.

2. *Symmetry of low-temperature* $CaSiO_3$

Experiments[8,9] indicate a tetragonal low-temperature structure with $c/a=0.993$ at 100 GPa[9] in apparent contrast to theoretical results, which give structures with $c/a=1.012$ (0 GPa) to 1.016 (150 GPa).[11,17] To resolve this question, we performed MD quenches at 100 GPa, where temperature was continuously lowered from 2500 K to 0 K and which at the end gave a new structure. Three cell shapes were used: cubic ($c/a=1$), tetragonal with $c/a=0.993$, and tetragonal with $c/a=1.014$. For fast quenching ($dT/dt=-6\times10^{14}$ K/s) in all cell shapes the resulting structure had the *Imma* symmetry. For slower quenching ($dT/dt=-3\times10^{14}$ K/s) and at the same time imposing $c/a=1.014$ the resulting structure had $I4/mcm$ symmetry (see Fig. 4 and Table II).[32]

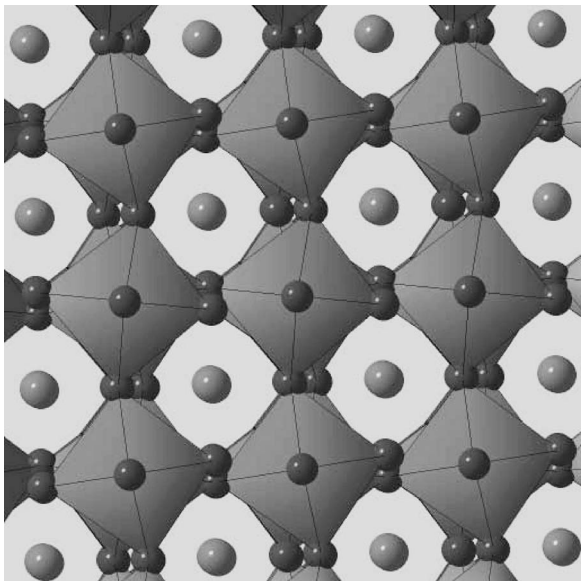

FIG. 4. The $I4/mcm$ structure along the fourfold axis of octahedra, where tilting takes place. This structure has only one tilting axis. (For better visibility tilting is exaggerated compared to an energetically optimized $CaSiO_3$ perovskite structure by a factor of 2.)

TABLE I. Structure of orthorhombic *Imma* $CaSiO_3$ perovskite at $P=100$ GPa and $T=0$ K. Lattice parameters: $a=4.6603$ Å, $b=6.5684$ Å, and $c=4.6997$ Å. (Lattice parameters at $P=40$ GPa and $T=0$ K: $a=4.8651$ Å, $b=6.8579$ Å, $c=4.8882$ Å.)

Atom type	Wykoff position	Coordinates
Ca	4*e*	$0,\frac{1}{4},0.4999$
Si	4*a*	0,0,0
O_1	4*e*	$0,\frac{1}{4},0.0401$
O_2	8*g*	$\frac{1}{4},0.0205,\frac{1}{4}$

Additionally 104 structural optimizations were performed to search for possible ground state structures. The starting tilting system for the octahedra was $\alpha^-\alpha^-\alpha^-$ with $a=5°$.[33] Lattice parameters of the 20-atom cell corresponding to a pressure of 100 GPa were slightly distorted to give c/a ratios of 0.986 and 1.014 and unit cell angles α, β, and γ taking values of 88°, 89°, 90°, 91°, and 92°. The same tilting system was combined with all nonequivalent combinations of lattice parameters. The optimizations consisted of two steps. In the first step, the lattice parameters were fixed and the atomic positions were relaxed. In the second step, the lattice parameters were also relaxed. 100 of the resulting structures had the $I4/mcm$ symmetry, and four had the *Imma*. The $I4/mcm$ is clearly preferred for $CaSiO_3$ perovskite at 0 K, since it has a lower enthalpy.

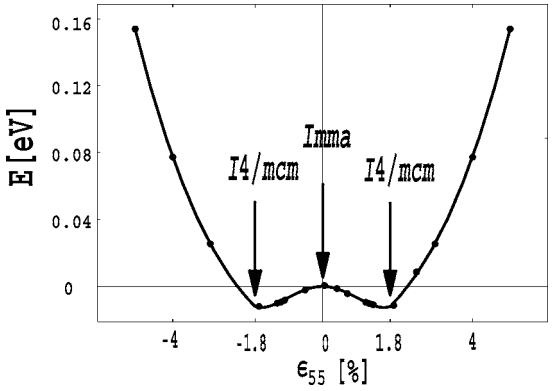

FIG. 5. Shear deformation of the *Imma* structure, tilting system $\alpha^0\beta^-\beta^-$. In this series of calculations the *Imma* structure parameters were changed by the imposed ε_{55} strain under fixed volume ($V=143.68$ Å^3). With given lattice parameters, the ionic positions were relaxed. Octahedral rotations turn out to be coupled to the deformation. At $|\varepsilon_{55}|=1.8\%$, the tilting system of the octahedra and the lattice parameters of the structure correspond to those of the $I4/mcm$ structure ($\alpha^0\beta^0\gamma^-$), to which the *Imma* structure transforms after imposition of any small ε_{55} shear followed by full structure optimization. This configuration corresponds to a minimum of the total energy. The tilting system for $\varepsilon_{55}=1.8\%$ is $\alpha^0\beta^0\gamma^-$ whereas for $\varepsilon_{55}=-1.8$, it is $\alpha^0\beta^-\gamma^0$. The energy barrier to overcome is 0.017 eV (per 20 atoms) and corresponds to 200 K, which means that the *Imma* structure can be stabilized by thermal vibrations above ~200 K.

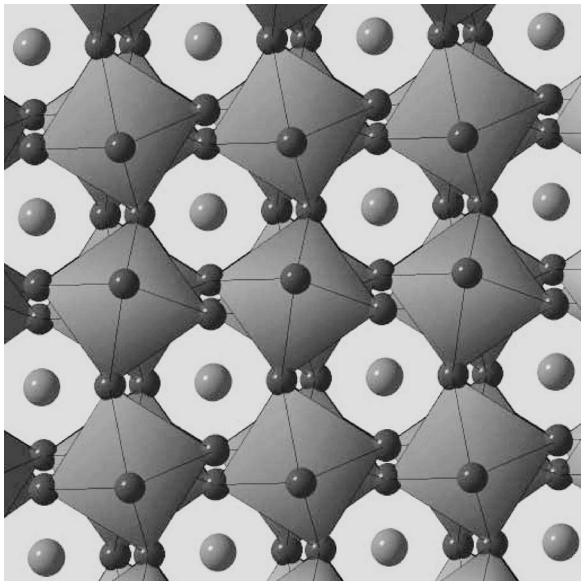

FIG. 6. The *Imma* structure along one of the tilting axes. This structure has two tilting axes (for better visibility tilting is exaggerated relative to an energetically optimized $CaSiO_3$ perovskite structure by a factor of 2).

Elastic constants calculations show that the *Imma* structure is mechanically unstable. Figure 5 shows the total energy surface in the vicinity of the *Imma* structure. Although the *Imma* structure corresponds to a saddle point of the energy and therefore is unstable at 0 K, it could be entropically stabilized at higher temperatures. This stabilization requires thermal energy to be greater than the energy barrier between the two energy wells shown in Fig. 5; this condition is already fulfilled at room temperature. The *Imma* structure could explain the different findings in experiment and in calculations—present for the past ten years—since it has $c/a<1$ (see Fig. 6 and Table I).

With the program POWDER CELL[34] we have generated diffraction patterns of different structures. We find that the *Imma* structure—unlike *I*4/*mcm*, *Pbnm* and *Pm*3*m*—explains peak intensities between $2\theta \in (14°, 15°)$ as shown in Fig. 7. These peaks have been used as diagnostic for the low-temperature distortion of $CaSiO_3$ perovskite.[4,8,9] Since in the *Imma* the difference between a and b is small, the diffraction pattern is pseudotetragonal. This explains why experiments[4,8,9] could be interpreted as observations of a tetragonal phase with $c/a<1$.

TABLE II. Structure of tetragonal *I*4/*mcm* $CaSiO_3$ perovskite at $P=100$ GPa and $T=0$ K. Lattice parameters: $a=b=4.6397$ Å and $c=6.6809$ Å. (Lattice parameters at $P=40$ GPa and $T=0$ K: $a=b=4.8463$ Å, $c=6.9433$ Å.)

Atom type	Wykoff position	Coordinates
Ca	4*b*	$0, \frac{1}{2}, \frac{1}{4}$
Si	4*c*	0,0,0
O_1	4*a*	$0, 0, \frac{1}{4}$
O_2	8*h*	0.2188, 0.7188,0

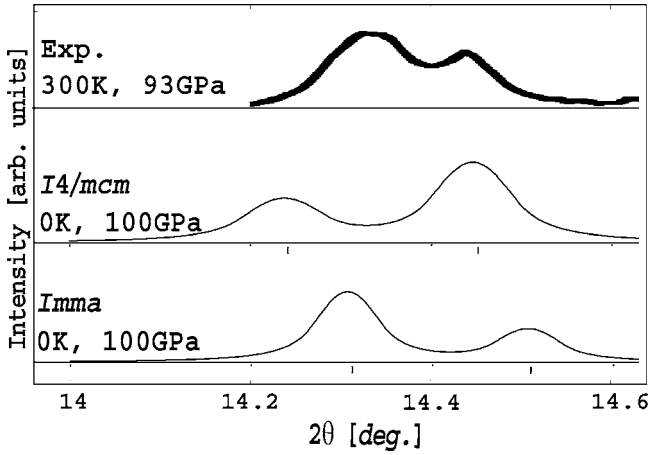

FIG. 7. Comparison of powder diffraction patterns of the simulated structure with experiment. Experimental intensities cannot be explained with the *I*4/*mcm* symmetry (X-ray wavelength $\lambda=0.413$ Å was used).

B. Thermal equation of state and anharmonic effects

The Grüneisen parameter γ is an important quantity in geophysics. This dimensionless parameter varies slowly as a function of pressure and temperature and occurs in equations that describe the thermoelastic behavior of materials—for example, in the equation describing temperature increase in adiabatic compression

$$\left(\frac{\partial \ln T}{\partial \ln \rho}\right)_S = \gamma, \tag{3}$$

where ρ is the density and S the entropy.

The value of γ is used to place constraints on the pressure and temperature dependence of the thermal properties of the Earth's mantle and core, the adiabatic temperature gradient and the reduction of shock-wave Hugoniots to room temperature. It has several definitions, e.g., it can be defined through thermal expansion α and heat capacity C_V

$$\alpha = \gamma_\alpha \frac{C_V}{K_T \cdot V}. \tag{4}$$

Alternatively, it can be defined through thermal pressure within the Mie-Grüneisen equation of state

$$P_{vib} = \frac{E_{vib}}{V}\gamma_p, \tag{5}$$

where E_{vib} is the vibrational energy. These two definitions (γ_α and γ_p) are identical for classical quasiharmonic solids. Quantum effects and intrinsic anharmonicity introduce (usually small) differences and an explicit dependence on temperature.

Following Ref. 30 we have calculated γ_{eff} in the form (2), from which we have extracted the temperature-dependent anharmonic and the temperature-independent (γ_{qh}, quasiharmonic) part of the Grüneisen parameter, using the formula:[30]

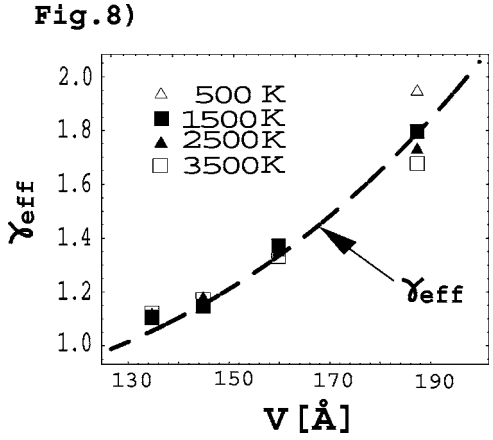

FIG. 8. Effective Grüneisen parameter in $CaSiO_3$. Best fit for $\gamma_{\mathrm{eff}}(V)$ depending only on volume in the form (7) is obtained with $\gamma_\infty=0.9185$, $\gamma_0=1.873$, $\beta=4.580$.

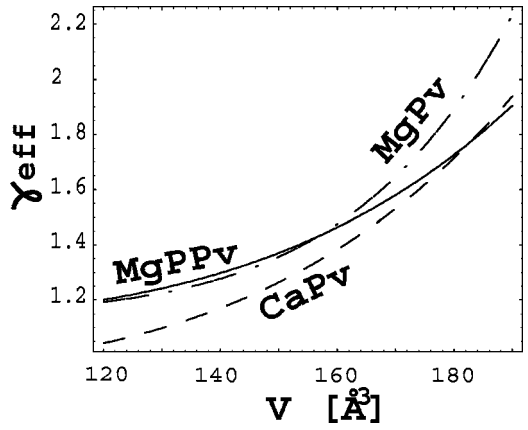

FIG. 9. Comparison of Grüneisen parameters of $CaSiO_3$ perovskite (CaPv), $MgSiO_3$ perovskite (MgPv), and $MgSiO_3$ post-perovskite (MgPPv).

$$\gamma_{eff}(V,T) = \gamma_{qh}(V) - \frac{1}{2}a(V)\frac{d\ln a}{d\ln V}T. \tag{6}$$

Following Zharkov and Kalinin,[35] we have assumed the simplest volume dependence of the intrinsic anharmonicity parameter a, $a=a_0x^m$, where $x=V/V_0$.

The volume dependence of the Grüneisen parameter is represented by a function proposed by Al'tshuler and Vorobev,[36,37]

$$\gamma_{eff}(V) = \gamma_\infty - (\gamma_\infty - \gamma_0)(V/V_0)^\beta, \tag{7}$$

where γ_0 and γ_∞ are the values of the Grüneisen parameter at ambient conditions ($V/V_0=1$, $V_0=187.31$ Å^3) and infinite compression, respectively. The temperature- and volume-dependent Grüneisen parameter then has five parameters γ_∞, γ_0, a_0, β, and m. Fitting them to data from 14 MD runs, we obtain $\gamma_\infty=0.9185$, $\gamma_0=1.873$, $a_0=1.29\times10^{-5}$ K^{-1}, $\beta=4.580$, $m=5.63$.[38] The Grüneisen parameter is higher than reported in the previous work.[39] The error on the a parameter is 15%. From our results, we see that at low pressures the effective Grüneisen parameter significantly depends on temperature, but this dependence (which is due to intrinsic anharmonicity) is suppressed at high pressure (Fig. 8).

For infinite compression $\gamma_\infty=2/3$ or $\gamma_\infty=1/2$ is expected, depending if—at infinite compression—we consider matter as an electron gas or a two-component plasma of electrons and protons, respectively. None of these values are comparable with the values we obtained, for two reasons: first, in our approach γ_∞ is just a fitted parameter; second there must be a phase transition to a metallic state before the volume limit ($V\to0$) is reached, which would be related to a discontinuous change in the Grüneisen parameter.

The intrinsic anharmonicity parameter a is related to the overall change of phonon frequencies ω_i with temperature at constant volume, $a=\left\langle\left(\frac{\partial\ln\omega_i}{\partial T}\right)_V\right\rangle$, and its positive value implies an overall increase of frequencies with temperature if the volume is kept fixed. Intrinsic anharmonic effects often (also in the case of $CaSiO_3$ perovskite) suppress dynamical instabilities at high T;[40] as a result, the cubic phase (dynamically unstable at low temperatures) is stabilized at high temperatures. Figure 9 compares the Grüneisen parameters of $MgSiO_3$ perovskite,[21,41] $MgSiO_3$ post-perovskite,[42] and $CaSiO_3$ perovskite. For all three materials, the effective Grüneisen parameters are given, which were obtained in a fitting procedure to γ_{eff} in a broad temperature range; at these conditions γ_{eff} is very close to γ_p.

C. Diffusion in $CaSiO_3$

Satellite measurements show a conductivity of $\sim10^2$ S/m for the lower mantle.[19] Ionic conductivity of this order implies fast ionic diffusion, as we show below. The electrical conductivity is given by the Nernst-Einstein relation,[43]

$$\sigma = \frac{nq^2}{k_BT}D, \tag{8}$$

where n is the concentration of the charge carriers, q their charge, and D the diffusion coefficient. In a system with average hopping time t and average hopping distance A, the diffusion coefficient is given by[43]

$$D = \frac{A^2}{2t}. \tag{9}$$

We combine these two relations to compute an expected hopping time t for a given conductivity

$$t = \frac{nq^2A^2}{2k_BT\sigma}. \tag{10}$$

We assume that in $CaSiO_3$ perovskite diffusion occurs by hopping of O^{2-} ions ($q=-2$) into a neighboring O^{2-} vacancy at a distance $A=2.35$ Å and that all Al^{3+} (~4 mol %) impurities are charge compensated by oxygen vacancies ($n_{O^{2-}}\simeq2$ mol %). The expected hopping time at 3500 K and 100 GPa is 0.28 ps, short enough to be observed in MD simulations. Note that with more realistic (much lower) vacancy concentrations even shorter hopping times would result. To enhance diffusion we remove an oxygen O^{2-} ion and apply a charge-compensating background. No diffusion has

been observed during the whole run of 8.2 ps. We can therefore rule out fast diffusion in cubic $CaSiO_3$ perovskite, although slow diffusion on longer time scales cannot presently be ruled out. $MgSiO_3$ post-perovskite was recently suggested to be an ionic conductor, which could explain high electrical conductivity of the D″ layer.[42] Other explanations for the observed high electrical conductivity of the lower mantle include ionic diffusion along grain boundaries and a possible electronic component, e.g., due to electron hopping between Fe sites in $(Mg,Fe)SiO_3$ perovskite or post-perovskite.

IV. DISCUSSION

We conclude that the enthalpy of the tetragonal $I4/mcm$ structure of $CaSiO_3$ perovskite at 0 K is lower than for any structure that has been proposed as the low-temperature structure for $CaSiO_3$ perovskite. Therefore, $I4/mcm$ is the most probable low-temperature symmetry. It was obtained from MD quenches and systematic scanning of the possible perovskite structures. Yet another structure was found from simulated quenching and systematic scanning. It has the *Imma* symmetry and—though mechanically unstable at 0 K—could be entropically stabilized at room temperature. The *Imma* structure reproduces experimental X-ray intensities. Note that experimental results could not be explained with the $I4/mcm$ symmetry.

We can now better understand the reasons for the contradictions between different calculations and experiment. Calculations of Akber-Knutson[12] were not strictly *ab initio*, and those of Magyari-Köpe[13] were based on linear muffin-tin methodology that may not be ideal for treating silicates; these works found the *Pbnm* structure to be the most stable. Warren *et al.*[14] and Wentzcovitch *et al.*[15] used pseudopotentials and found no deviation from cubic symmetry, but it is well known that the derivation of pseudopotentials—especially for such elements as Ca—may be difficult (problems due to semicore states, etc.). We believe that the most accurate calculations are those of Refs. 11, 16, and 17, consistent among each other and showing that the $\alpha^0\beta^0\gamma^-$ ($I4/mcm$ tetragonal) is the energetically most favorable configuration.

Reference 16 finds a c/a ratio <1 for the *Imma* structure but makes no connection to experimental observations. We show that there is a possibility for the thermal stabilization of the orthorhombic (pseudotetragonal) *Imma* structure and that it easily explains the experimental diffraction pattern, while its enthalpy is only 0.85 meV/atom higher than that of the $I4/mcm$ structure at 100 GPa and 0 K.

Phase transition between the cubic phase of $CaSiO_3$ perovskite and the low temperature phase takes place at around 1000–2000 K. This indicates that it is the cubic phase of $CaSiO_3$ perovskite that is present in the lower mantle due to high temperatures in the mantle.

We did not observe any fast ionic diffusion in $CaSiO_3$ perovskite. The origin of the high electrical conductivity of the mantle could be in ionic transport at grain boundaries or in the ionic or electronic components from $(Mg,Fe)SiO_3$ perovskite and post-perovskite.[42,44,45]

As can be seen from the various questions—concerning symmetry, diffusion, effects of temperature, equation of state—a cross-check between experiment and theory always plays an important role in high-pressure research. The reader is referred to recent articles by Oganov and Ono (Refs. 42, 46, and 47) where the strong interplay between theory and experiment led to the finding of new phases of $MgSiO_3$ and Al_2O_3 with the $CaIrO_3$-type structure. In this study, *ab initio* calculations helped to elucidate the nature of the experimentally observed low-T phase of $CaSiO_3$ perovskite.

ACKNOWLEDGMENTS

We are grateful to T. Racic for computational assistance, D.Y. Jung for communication of results of static optimizations and technical help, A. Garcia and S. Ono for extremely useful discussions, and Mario Valle for visualization. We thank CSCS (Manno) and ETH Zurich for computational facilities and for funding (Grant No. TH-27033).

*E-mail address: donat.adams@mat.ethz.ch

[1] G. Fiquet, Z. Kristallogr. **216**, 248 (2001).
[2] T. Irifune, Nature **370**, 131 (1994).
[3] S.-H. Shim, T. S. Duffy, and G. Shen, J. Geophys. Res. **105**, 25955 (2000).
[4] S.-H. Shim, T. S. Duffy, and G. Shen, Phys. Earth Planet. Inter. **120**, 327 (2000).
[5] H. K. Mao, L. C. Chen, R. J. Hemley, A. P. Jephcoat, and Y. Wu, J. Geophys. Res. **94**, 17889 (1989).
[6] Y. Wang, D. J. Weidner, and F. Guyot, J. Geophys. Res. **98**, 19795 (1996).
[7] L.-G. Liu and A. E. Ringwood, Earth Planet. Sci. Lett. **28**, 209 (1975).
[8] S.-H. Shim, R. Jeanloz, and T. S. Duffy, Geophys. Res. Lett. **29**, 19 (2002).
[9] S. Ono, Y. Ohishi, and K. Mibe, Am. Mineral. **89**, 1480 (2004).
[10] T. Kurashina, K. Hirose, S. Ono, N. Sata, and Y. Ohishi, Phys. Earth Planet. Inter. **145**, 67 (2004).
[11] L. Stixrude, R. Cohen, R. Yu, and H. Krakauer, Am. Mineral. **81**, 1293 (1996).
[12] S. Akber-Knutson, M. S. T. Bukowinski, and J. Matas, Geophys. Res. Lett. **29**, 4 (2002).
[13] B. Magyari-Köpe, L. Vitos, G. Grimvall, B. Johansson, and J. Kollar, Phys. Rev. B **65**, 193107 (2002).
[14] M. C. Warren, G. J. Ackland, B. B. Karki, and S. J. Clark, Miner. Mag. **62**, 585 (1998).
[15] R. M. Wentzcovitch, N. L. Ross, and G. D. Price, Phys. Earth Planet. Inter. **90**, 101 (1995).
[16] R. Caracas, R. Wentzcovitch, G. D. Price, and J. P. Brodhold, Geophys. Res. Lett. **32**, 146 (2005).
[17] D. Y. Jung and A. R. Oganov, Phys. Chem. Miner. **32**, 146 (2005).
[18] While the ideal perovskite structure is cubic (lattice constants a_0, b_0, c_0), the *Imma* and $I4/mcm$ have a tetragonal unit cell with

lattice constants $a, b \sim 2a_0$, and $c \sim \sqrt{2} \cdot c_0$. Through the inverse of this transformation, we compute the lattice parameters of the cubic subcell.

[19] S. Constable and C. Constable, Geochem., Geophys., Geosyst. DOI 10.1029/2003GC000634 **5**, Q01006 (2004).

[20] M. Matsui and G. D. Price, Nature **351**, 735 (1991).

[21] A. R. Oganov, J. P. Brodholt, and G. D. Price, Nature **411**, 934 (2001).

[22] G. Kresse and J. Furthmüller, Phys. Rev. B **54**, 11169 (1996).

[23] J. P. Perdew, K. Burke, and M. Ernzerhof, Phys. Rev. Lett. **77**, 3865 (1996).

[24] P. E. Blöchl, Phys. Rev. B **50**, 17953 (1994).

[25] P. E. Blöchl, C. J. Först, and J. Schimpl, Bull. Mater. Sci. **26**, 33 (2003).

[26] G. Kresse and D. Joubert, Phys. Rev. B **59**, 1758 (1999).

[27] S. Nosé and M. L. Klein, J. Chem. Phys. **78**, 6928 (1983).

[28] M. P. Allen and D. J. Tildesley, *Computer Simulations of Liquids* (Oxford Science Publications, Oxford, 1987).

[29] L. Vocadlo, D. Alfè, I. G. Wood, J. P. Brodholt, and G. D. Price, Nature **423**, 235 (2003).

[30] A. R. Oganov and P. I. Dorogokupets, Phys. Rev. B **67**, 224110 (2003).

[31] Tilting angles were derived from Si-O-Si bond angles projected onto the plane perpendicular to the tilting axis.

[32] The slower quenching rate combined with $c/a=1$ and $c/a=0.993$ resulted in a structure with the *Imma* symmetry.

[33] This tilting system in the case of rigid octahedra has space group $R3c$. In our calculations the octahedra were tilted and distorted. The distortion originates in the distortion of the unit cell.

[34] W. Kraus and G. Nolze (Bundesanstalt fuer Materialforschung und -prüfung, 1996).

[35] V. N. Zharkov and V. A. Kalinin, *Equation of State of Solids at High Pressures and Temperatures* (Consultant Bureau, New York, 1971).

[36] L. V. Al'tshuler, S. E. Brusnikin, and E. A. Kuzmenkov, J. Appl. Mech. Tech. Phys. **161**, 134 (1987).

[37] V. S. Vorobev, High Temp. - High Press. **34**, 391 (1996).

[38] We excluded two data points at lowest temperature (500 K) and highest pressures (100 GPa, 150 GPa). At these conditions the structure has large deviations from cubic, whereas here we determine the characteristics of the cubic structure.

[39] L. Li, D. J. Weidner, J. P. Brodholt, D. Alfé, G. D. Price, R. Caracas, and R. Wentzcovitch, EOS Trans. Am. Geophys. Union **86**, T21C (2005).

[40] M. T. Dove, *Introduction to Lattice Dynamics* (Cambridge University Press, Cambridge, England, 1993).

[41] A. R. Oganov, J. P. Brodholt, and G. D. Price, Earth Planet. Sci. Lett. **184**, 555 (2001).

[42] S. Ono and A. R. Oganov, Earth Planet. Sci. Lett. **236**, 914 (2005).

[43] S. Elliott, *The Physics and Chemistry of Solids* (Wiley & Sons, Chichester, 1998).

[44] C. McCammon, M. Hutchison, and J. Harris, Science **278**, 434 (1997).

[45] N. C. Richmond and J. P. Brodholt, Am. Mineral. **83**, 947 (1998).

[46] A. R. Oganov and S. Ono, Nature **430**, 445 (2004).

[47] A. R. Oganov and S. Ono, Proc. Natl. Acad. Sci. U.S.A. **102**, 10828 (2005).